What KM3-230213A event may tell us about the neutrino mass and dark matter

Basabendu Barman,[1,*] Arindam Das,[2,3,†] and Prantik Sarmah[4,‡]

[1]*Department of Physics, School of Engineering and Sciences, SRM University-AP, Amaravati 522240, India*

[2]*Institute for the Advancement of Higher Education, Hokkaido University, Sapporo 060-0817, Japan*

[3]*Department of Physics, Hokkaido University, Sapporo 060-0810, Japan*

[4]*Institute of High Energy Physics, Chinese Academy of Sciences, Beijing, 100049, People's Republic of China*

(Received 13 April 2025; accepted 10 September 2025; published 6 October 2025)

Within the general $U(1)$ scenario, we demonstrate that the ultrahigh-energy neutrinos recently detected by KM3NeT could originate from a decaying right-handed neutrino dark matter, with a mass of 440 PeV. Considering dark matter production via freeze-in, we delineate the parameter space that satisfies the observed relic abundance and also lies within the reach of multiple gravitational wave detectors. Our study provides a testable new physics scenario, enabled by multimessenger astronomy.

DOI: 10.1103/t58k-sjq5

I. INTRODUCTION

The KM3NeT experiment recently reported the detection of event KM3-230213A [1], involving ultrahigh-energy (UHE) neutrinos in the range 110 PeV $\leq E_\nu \leq$ 790 PeV, with a median energy of 220 PeV—the highest-energy neutrino observed on Earth to date. The experiment detected an UHE muon through its deep-sea neutrino telescope, with an energy of 120^{+110}_{-60} PeV, arriving from an almost horizontal direction (RA: 94.3°, Dec: −7.8°). This muon is believed to have originated from a more energetic neutrino interacting near the detector. Such energetic neutrinos can be produced in cosmic-ray interactions, specifically via proton-proton and proton-photon collisions at standard astrophysical sources, where emission of photons associated with neutrinos is guaranteed. However, no such energetic source is known to exist within the Milky Way or nearby galaxies. The absence of compelling evidence pinpointing the origin of these UHE neutrinos, as observed by KM3NeT [2–4], raises the possibility that they have a cosmogenic origin. In particular, they could be produced via the Greisen-Zatsepin-Kuzmin effect [5,6], in association with UHE gamma rays, as predicted in various models [7–10]. However, the large uncertainty in the flux of event KM3-230213A—of the order of $\mathcal{O}(3)$—not only exceeds expectations from current UHE neutrino and gamma-ray flux models, but also surpasses the sensitivities of IceCube and the Pierre Auger Observatory (PAO), where no similar event has been observed within a 2.5σ–3σ significance range. This discrepancy challenges the cosmogenic neutrino hypothesis [11,12] and calls for other possible explanations.

In [13], we investigated a decaying dark matter (DM) scenario to explain the origin of UHE neutrinos observed by IceCube. The detection of KM3NeT events prompts us to reconsider this framework.[1] Our scenario can be naturally embedded within a general anomaly-free $U(1)$ extension of the Standard Model (SM), incorporating three singlet right-handed neutrinos (RHNs) [32,33] and a beyond-the-Standard-Model (BSM) scalar singlet. The BSM scalar acquires a nonzero vacuum expectation value (VEV), breaking the $U(1)_X$ symmetry and generating Majorana masses for the RHNs, thereby inducing the seesaw mechanism. It gives rise to tiny neutrino masses and flavor mixing [34–40]. We consider a long-lived decaying DM candidate, that can be identified as the lightest RHN with a mass in the PeV range, depending on the neutrino mass hierarchy—either normal (NH) or inverted (IH). By fitting neutrino oscillation data [41], we estimate the DM lifetime for both NH and IH cases and use this to reproduce the expected neutrino and photon fluxes at KM3NeT [2–4]. This PeV-scale decaying DM, which explains the origin of the UHE neutrino event with $\langle E_\nu \rangle \simeq 220$ PeV, could be produced via the freeze-in

*Contact author: basabendu.b@srmap.edu.in

†Contact author: arindamdas@oia.hokudai.ac.jp

‡Contact author: prantiksarmah@ihep.ac.cn

Published by the American Physical Society under the terms of the Creative Commons Attribution 4.0 International license. Further distribution of this work must maintain attribution to the author(s) and the published article's title, journal citation, and DOI. Funded by SCOAP³.

[1]Other possible new physics explanation for KM3NeT events can be found in [14–31].

mechanism [42]. Interestingly, in [43], the authors argued that if the Universe is in its preferred CPT-symmetric vacuum, then such a PeV-scale DM naturally emerges from the big bang like Hawking radiation from a black hole. The breaking of $U(1)_X$ symmetry also leads to the formation of one-dimensional topological defects in the form of cosmic strings (CSs) [44,45], characterized by a string tension $G\mu \sim \mathbb{B}Gv_\Phi^2$, where v_Φ is the VEV of the $U(1)_X$ symmetry-breaking singlet scalar and $\mathbb{B} \sim 0.1$ [46–48]. Thus, this scenario provides a compelling framework in which the KM3NeT event not only provides a hint toward decaying DM, but sheds light on the neutrino mass hierarchy as well. Moreover, the gravitational waves (GWs) from cosmic strings predicted in this scenario could be probed by several proposed GW detectors. Finally, we constrain very heavy Z', that acquires mass via spontaneous breaking of $U(1)_X$ from KM3-230213A events and DM abundance and GW from CSs. Such heavy gauge bosons are beyond the scope of existing direct search experiments.

II. THE MODEL FRAMEWORK

Under the SM $\otimes$ $U(1)_X$ gauge symmetry, the SM quarks transform as $q_L^i = \{3, 2, \frac{1}{6}, \frac{1}{6}x_H + \frac{1}{3}x_\Phi\}$, $u_R^i = \{3, 1, \frac{2}{3}, \frac{2}{3}x_H + \frac{1}{3}x_\Phi\}$, and $d_R^i = \{3, 1, -\frac{1}{3}, -\frac{1}{3}x_H + \frac{1}{3}x_\Phi\}$, respectively. The SM leptons transform as $\ell_L^i = \{1, 2, -\frac{1}{2}, -\frac{1}{2}x_H - x_\Phi\}$ and $e_R^i = \{1, 1, -1, -x_H - x_\Phi\}$, respectively, while the SM Higgs transforms as $H = \{1, 2, \frac{1}{2}, \frac{x_H}{2}\}$ with $\{x_H, x_\Phi\} \in \mathrm{Re}$. Three SM-singlet RHNs, required to cancel gauge and mixed gauge-gravity anomalies, transform as $N_R^i = \{1, 1, 0, -x_\Phi\}$ with $i = 1$, 2, 3 and one SM-singlet $U(1)_X$ scalar transforms as $\Phi = \{1, 1, 0, 2x_\Phi\}$. The Yukawa interactions relevant for the neutrino mass can be written as

$$\mathcal{L} \supset -Y_{\nu_{\alpha\beta}} \overline{\ell_L^\alpha} \tilde{H} N_R^\beta - \frac{1}{2} Y_{N_\beta} \Phi \overline{(N_R^\beta)^c} N_R^\beta + \mathrm{H.c.}, \quad (1)$$

where we consider a basis where Y_{N_α} is a diagonal matrix and $\tilde{H} = i\tau^2 H^*$ with τ^2 being the second Pauli matrix. The scalar potential of this scenario is given by

$$V = \sum_{\mathcal{I}=H,\Phi} [m_\mathcal{I}^2 (\mathcal{I}^\dagger \mathcal{I}) + \lambda_\mathcal{I} (\mathcal{I}^\dagger \mathcal{I})^2] + \lambda_{\mathrm{mix}} (H^\dagger H)(\Phi^\dagger \Phi). \quad (2)$$

After the breaking of $U(1)_X$ and electroweak gauge symmetries, the scalar fields H and Φ develop their VEVs as

$$\langle H \rangle = \frac{1}{\sqrt{2}} \begin{pmatrix} v + h \\ 0 \end{pmatrix} \quad \text{and} \quad \langle \Phi \rangle = \frac{v_\Phi + \phi}{\sqrt{2}}, \quad (3)$$

where electroweak scale is $v = 246$ GeV at the potential minimum. In the limit $v_\Phi \gg v$, the mass of the $U(1)_X$ gauge boson can be written as $M_{Z'} = 2g_X x_\Phi v_\Phi$. Taking $x_\Phi = 1$ without the loss of generality, we find that for $x_H = -2$ ℓ_L and q_L do not have interactions with Z', for $x_H = 0$ left- and right-handed SM fermions interact equally with Z' which provides the B-L scenario, and finally for $x_H = -1$ e_R does not interact with Z'. The breaking of $U(1)_X$ and electroweak symmetries induce the Majorana and Dirac mass terms for RHNs and light left-handed neutrinos from Eq. (1) as

$$M_{N_\beta} = \frac{Y_{N_\beta}}{\sqrt{2}} v_\Phi, \qquad m_{D_{\alpha\beta}} = \frac{Y_{\nu_{\alpha\beta}}}{\sqrt{2}} v. \quad (4)$$

Hence light active neutrino masses follow the seesaw formula

$$m_\nu \simeq -m_D M_N^{-1} m_D^T, \quad (5)$$

explaining the origin of tiny neutrino masses and flavor mixing. Diagonalizing Eq. (5) one obtains

$$\mathcal{U}^T m_\nu \mathcal{U} = \mathrm{diag}(m_1, m_2, m_3), \quad (6)$$

where $\mathcal{U}$ is the Pontecorvo-Maki-Nakagawa-Sakata (PMNS) matrix and it depends on neutrino oscillation data [41]. We consider the light neutrino mass eigenvalues follow $m_1 = m_{\mathrm{lightest}} < m_2 < m_3$ in NH and $m_3 = m_{\mathrm{lightest}} < m_1 < m_2$ in IH cases where m_{lightest} is the lightest light neutrino mass being a very small free parameter (see Appendix A for details). From the seesaw formula we write

$$V_{\alpha\beta}^{\mathrm{NH(IH)}} = \mathcal{U}^* \sqrt{D^{\mathrm{NH(IH)}}} \sqrt{M_N^{-1}}, \quad (7)$$

when M_N is in diagonal basis for NH (IH) case. From the definition of neutrino mixing we obtain

$$V_{\alpha\beta}^{\mathrm{NH(IH)}} = m_{D_{\alpha\beta}}^{\mathrm{NH(IH)}} / M_{N_\beta} = \frac{Y_{\nu_{\alpha\beta}}^{\mathrm{NH(IH)}} v}{\sqrt{2} M_{N_\beta}}. \quad (8)$$

Out of three RHN species, we identify the lightest RHN species [$N_{1(3)}$ in NH(IH)] as a long-lived decaying DM candidate ensured by the Yukawa coupling $Y_{\nu_{\alpha\beta}}^{\mathrm{NH(IH)}}$. Partial decay widths of very heavy RHNs [49] neglecting the masses of SM bosons are

$$\Gamma(N_\beta \to \ell_\alpha W) \simeq \frac{|Y_{\nu_{\alpha\beta}}^{\mathrm{NH(IH)}}|^2 M_{N_\beta}}{32\pi},$$
$$\Gamma(N_\beta \to \nu_\alpha Z) = \Gamma(N_\beta \to \nu_\alpha h) \simeq \frac{|Y_{\nu_{\alpha\beta}}^{\mathrm{NH(IH)}}|^2 M_{N_\beta}}{64\pi}, \quad (9)$$

while its radiative decay rate for $M_N >> M_W$ is given by

$$\Gamma_{N_\beta \to \nu_\alpha \gamma} \simeq M_{N_\beta} \frac{\alpha_{\mathrm{EM}} |Y_{\nu_{\alpha\beta}}^{\mathrm{NH(IH)}}|^2}{256\pi^6} \left(\frac{m_\mu}{v}\right)^2, \quad (10)$$

TABLE I. Benchmark values of active-sterile Yukawa coupling along with corresponding DM decay lifetime, for normal and inverted hierarchies. The DM mass is fixed to 440 PeV.

$Y_{21}^{\rm NH}$	$Y_{23}^{\rm IH}$	$\tau_{\rm DM}^{\rm NH}$ [s]	$\tau_{\rm DM}^{\rm IH}$ [s]
3.27×10^{-31}	1.22×10^{-30}	7×10^{29}	5×10^{28}

where $\alpha_{\rm EM}=1/137$ is the fine structure and Fermi constants, respectively. However, the radiative decay rate has a subdominant contribution to the total decay rate.

In the context of KM3-230213A, $N_{1(3)}$ could be a potential DM candidate for the NH (IH) case. The DM lifetime, including all possible two-body decays, reads

$$\tau_{\rm DM}^{\rm NH(IH)}\approx(7.5\times10^{30}\ {\rm s})\left(\frac{440\ {\rm PeV}}{M_{1(3)}}\right)\left(\sum_\alpha\left|\frac{Y_{\nu_{\alpha1(3)}}^{\rm NH(IH)}}{10^{-31}}\right|^2\right)^{-1}. \tag{11}$$

Fitting neutrino oscillation data [41] in Eqs. (7) and (8) we find Yukawa couplings $Y_{21}^{\rm NH}(Y_{23}^{\rm IH})\simeq3.27\times10^{-31}$ (1.22×10^{-30}) between $N_{1(3)}$ and ν_μ. We defined the lightest light neutrino mass as $m_{\rm lightest}=r\sqrt{\Delta m_{12}^2}=4.39\times10^{-65}$ (2.11×10^{-64}) GeV for NH (IH), where r is a tiny free parameter of benchmark values 5.03×10^{-54} (2.42×10^{-53}) for NH (IH) case. Using $Y_{21}^{\rm NH}$ $(Y_{23}^{\rm IH})$ in Eq. (11) we find $\tau_{\rm DM}^{\rm NH(IH)}=7\times10^{29}$ (5×10^{28}) s. The details of the benchmark pints chosen above are tabulated in Table I.

In Fig. 1 we show DM lifetime as a function of the Yukawa Y_ν, for the two benchmark points in Table I. Since $\Gamma_{\rm DM}\propto M_N|Y_\nu|^2$, hence a larger coupling requires smaller M_N to obtain a constant lifetime. It is crucial to mention that the long-lived RHN, which is a potential DM candidate, does not participate in the neutrino mass generation mechanism.

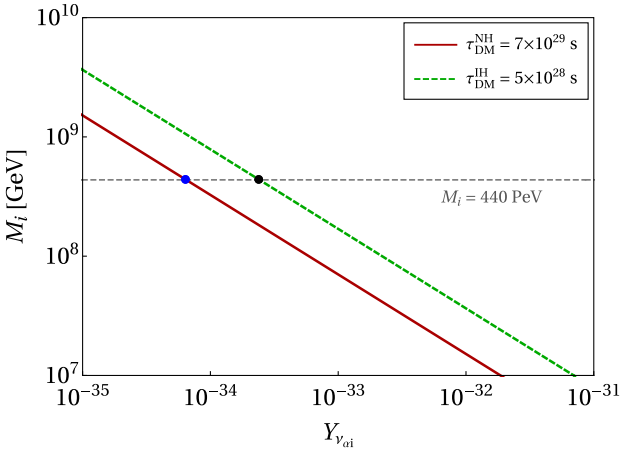


FIG. 1. Contours of DM lifetime, corresponding to normal (solid, red) and inverted (dashed, green) hierarchy. The blue and black points correspond to the Yukawas mentioned in Table I. The horizontal dashed line denotes the DM mass required to explain the KM3NeT event.

III. DARK-MATTER-INDUCED EXPLANATION OF THE EXCESS

The decay of $N_{1(3)}$ can yield high-energy gamma rays and neutrinos in the final state. To compute the flux of these secondaries from $N_{1(3)}$ in the Milky Way (MW), we choose the extensively explored Navarro-Frenk-White (NFW) [50,51] density profile of the Milky Way DM halo among many modes of DM profile [50–54]. As a function of the Galactocentric radius $(R_{\rm GC})$ the NFW profile becomes

$$\rho_{\rm DM}=\rho_{\rm NFW}(R_{\rm GC})=\frac{\rho_{\rm C}}{(R_{\rm GC}/R_{\rm C})(1+R_{\rm GC}/R_{\rm C})^2}, \tag{12}$$

where $R_{\rm C}=11$ kpc and $\rho_{\rm C}$ are the characteristic scale and density, respectively, where $\rho_{\rm C}$ is obtained by normalizing the DM profile to the DM density at solar neighborhood, $\rho_\odot=0.43\ {\rm GeV\,cm^{-3}}$. The flux of secondary gamma rays and neutrinos can be obtained by estimating the amount of DM in the angular region $\Delta\Omega$ of observation and given by

$$\mathcal{D}=\frac{1}{\Delta\Omega}\int_{\Delta\Omega}{\rm d}\Omega\int_0^{s_{\rm max}}{\rm d}s\rho_{\rm DM}(s,b,l). \tag{13}$$

Here, s is the line of sight distance which is connected to the Galactic longitude (l) and latitude (b) by the relation $r=\sqrt{s^2+R_\odot^2+2sR_\odot\cos b\,\cos l}$, where $R_\odot=8.3$ kpc is the distance to the Milky Way center from the Sun. The flux of the secondaries is given by

$$\frac{{\rm d}^2\phi_{i,{\rm G}}(E_i)}{{\rm d}E_i{\rm d}\Omega}=\frac{\mathcal{D}}{4\pi M_{\rm DM}\tau_{\rm DM}}\frac{{\rm d}N_i(E_i)}{{\rm d}E_i}, \tag{14}$$

where i represents gamma rays or neutrinos of any specific flavor. In addition to the Galactic DM, extra-Galactic DM can also contribute to the high-energy gamma-ray and neutrino fluxes, which can be obtained by the following formula:

$$\frac{d\phi_{i,{\rm EG}}(E_i)}{dE_i}=\frac{c\rho_{\rm DM}}{4\pi M_{\rm DM}\tau_{\rm DM}}\int dz\left|\frac{dt}{dz}\right|\frac{dN(E_i')}{dE_i'}e^{-\tau_{\rm OD}(E_i',z)}, \tag{15}$$

where $E_i'=E_i(1+z)$ corresponds to the energy of the ith particle at redshift z. The DM density is given by $\rho_{\rm DM}=\Omega_{\rm DM}\rho_c$, where $\rho_c=4.7\times10^{-6}\ {\rm GeV\,cm^{-3}}$ is the critical DM density in a flat Friedmann-Lemaître-Robertson-Walker universe and $\Omega_{\rm DM}=0.27$. The cosmological line element $|\frac{dt}{dz}|$ can be expressed as

$$\left|\frac{dt}{dz}\right|=\frac{1}{\mathcal{H}_0(1+z)\sqrt{(1+z)^3\Omega_{\rm m}+\Omega_\Lambda}}, \tag{16}$$

where $\Omega_m=0.315$, $\Omega_\Lambda=0.685$ and $\mathcal{H}_0=67.3\ {\rm km\,s^{-1}\,Mpc^{-1}}$ is the current expansion rate of the Universe. The factor

$e^{-\tau_{\rm OD}(E_i',z)}$ takes into account of the attenuation of the gamma-ray flux due to pair production losses in the extra-Galactic background light (EBL) and cosmic microwave background (CMB) during propagation, where $\tau_{\rm OD}(E_i', z)$ is the total optical depth of EBL and CMB. The optical depth (OD) of EBL is taken from [55]. The term dN_i/dE_i in Eqs. (14) and (15) represents differential spectra of secondary gamma rays and neutrinos as a function of energy E_i and obtained from HDMSpectra [56].

The total flux (ϕ_i), obtained by summing over both the Galactic and extra-Galactic components, depends on two free parameters: (i) the (decaying) DM mass $M_{\rm DM}$ being set at 440 PeV to kinematically allow the secondaries to acquire energy about 220 PeV from two-body decay and (ii) the DM lifetime $\tau_{\rm DM}$ where we consider gamma-ray observations by different telescopes across a broad energy band $(10^1$–$10^6)$ TeV. In the lower energies, $E_\gamma < 10^3$ TeV, we adopt the diffuse flux measurements from the inner Galactic plane ($15° < l < 125°$ and $-5° < b < 5°$) by the Kilometer Square Array at the Large High Altitude Air Shower Observatory (LHAASO-KM2A) [57]. For higher energies, we constrain the gamma-ray flux from DM decay using the upper limits on UHE photon flux from Moscow State University Extensive Air Shower (EAS-MSU) array [58] and Pierre Auger Observatory (PAO HECO + SD750) [59]. The gamma-ray flux calculated for the inner Galactic plane from the $N_{1(3)} \to \nu_\mu \gamma$ decay assuming NH (IH) is represented by the solid (dashed) purple curve in Fig. 2.

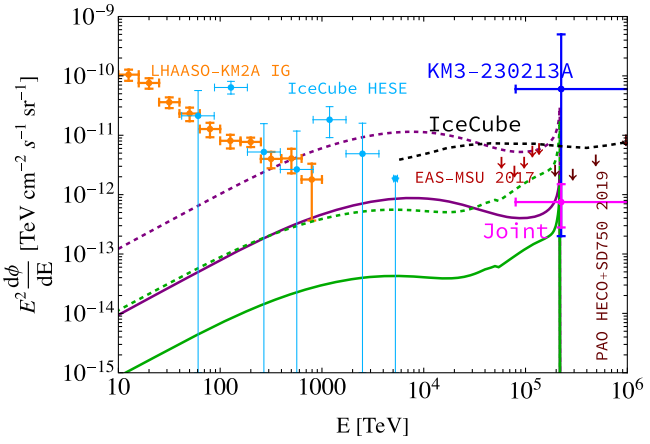


FIG. 2. Gamma-ray (dashed curve) and ν_μ (solid curve) fluxes for $\tau_{\rm DM} = 7 \times 10^{29}$ (in green, NH) and 5×10^{28} s (in purple, IH), respectively, considering $M_{\rm DM} = 440$ PeV. We compare our results with the fluxes from KM3NeT [1] event with 3σ error bars (blue), best fit flux from joint analysis of KM3NeT + IceCube + PAO (magenta), IceCube HESE [61] data (light blue), 90% CL sensitivity of IceCube [62] for cosmogenic neutrinos (black dotted), measurement of diffuse gamma rays from the inner Galactic (IG) plane by LHAASO [57] (orange), the upper limits on UHE gamma-ray flux by EAS-MSU [58] (maroon downward arrow), and PAO HECO + SD750 [59] (brown downward arrows), respectively.

For comparison, we include gamma-ray data from LHAASO-KM2A (orange), EAS-MSU (maroon downward arrows), and PAO HECO + SD750 (brown downward arrows). To remain consistent with these observations, $\tau_{\rm DM}^{\rm NH(IH)}$ is set to 7×10^{29} (5×10^{28}) s. The ν_μ flux from $N_{1(3)}$ decay, computed for the angular region constrained by the uncertainty in the arrival direction of KM3-230213A, is shown as the solid (dashed) green curve. We account for neutrino oscillations during propagation, leading to a final neutrino flavor ratio at Earth of 3:2:1 for NH and 1:2:3 for IH [60]. Consequently, the muon neutrino flux after oscillations remains similar in both cases. While the predicted neutrino flux is over an order of magnitude lower than the central flux value of the KM3-230213A event, it still lies within its 3σ uncertainty. Thus, a DM origin for the KM3-230213A event cannot be completely ruled out. For consistency with existing observations, we also display IceCube's high-energy starting events (HESE) [61] as cyan data points. While the resulting neutrino flux is close to the central value of KM3-230213A, the corresponding gamma-ray flux is in tension with the observed gamma-ray data. It is important to note that the choice of $\tau_{\rm DM}$ is not unique; by adjusting the Yukawa parametrization, one can fine-tune the gamma-ray flux to match observations.

We also estimate the expected number of muon neutrino events at KM3NeT for our predicted neutrino flux from DM decay. The number of events $N_{\rm event}$ in the energy interval ΔE_{ν_μ} is given by

$$N_{\rm event} = \mathcal{T}_{\rm obs} \int_{E_{\nu_\mu}}^{E_{\nu_\mu}+\Delta E_{\nu_\mu}} dE_{\nu_\mu} \frac{d\phi_{\nu_\mu}}{dE_{\nu_\mu}} \mathcal{A}_{\rm eff}(E_{\nu_\mu}), \quad (17)$$

where $\mathcal{T}_{\rm obs}$ is the observation time and $\mathcal{A}_{\rm eff}(E_{\nu_\mu})$ is the effective area of KM3NeT detector for muon neutrinos [63]. For the computation of the events, we consider the diffuse flux integrated over the entire Galactic DM halo. In the left panel of Fig. 3, we show the expected number of events (black line) as a function energy for a observation time of 10 years. The gray band shows the 1σ spread in the events considering Poisson statistics, i.e., $\sigma = \sqrt{N_{\rm event}}$. In addition, we show the variation of the total events integrated in the energy range 5–5×10^5 TeV with respect to $\tau_{\rm dm}$ in the right panel. The gray band corresponds to the 1σ uncertainty, and the red horizontal line corresponds to one event. As it is evident, KM3NeT will be able to probe $\tau_{\rm dm}$ up to around 10^{31} s after 10 years of observation.

It is important to mention that future detection of additional diffuse neutrinos by KM3NeT, IceCube, Auger, and upcoming experiments—such as IceCube-Gen2, GRAND, HUNT, and TRIDENT—could significantly reduce this uncertainty and help resolve the current tension. Indeed, a recent joint analysis [12] by the KM3NeT, IceCube, and PAO Collaborations has reported a revised flux estimate (magenta cross in Fig. 2) that is

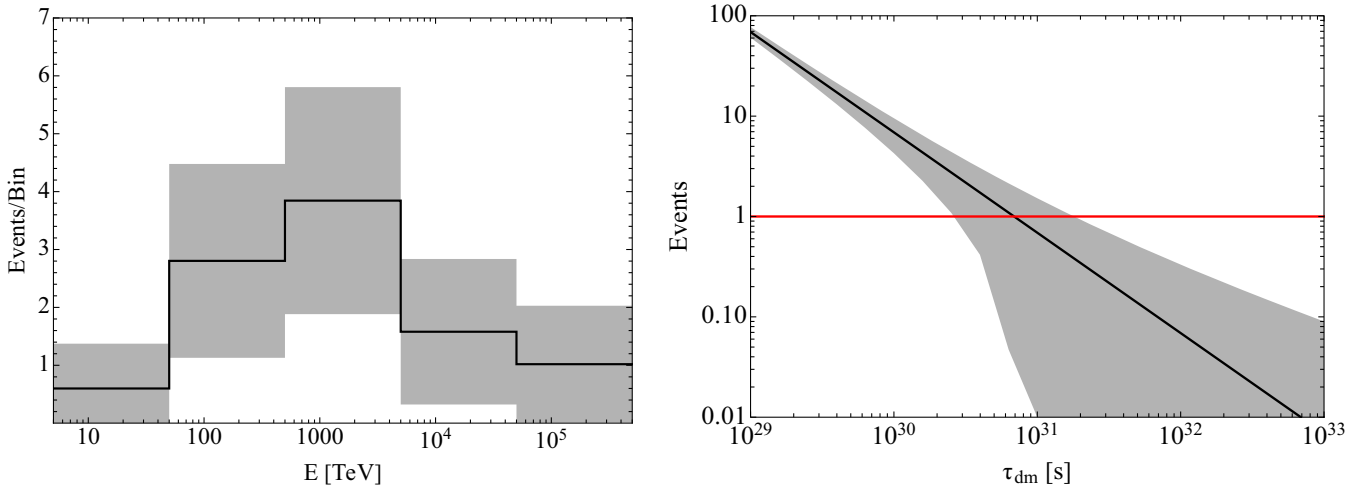


FIG. 3. Left: expected number of muon neutrino events in KM3NeT for an observation time of 10 years. Right: the gray band shows the 1σ uncertainty in the events in Poisson statistics. The red straight line parallel to the horizontal axis marks one event counted by KM3NeT.

approximately 2 orders of magnitude lower than the initial one. While this mitigates the discrepancy, a residual tension at the $(2.5\text{–}3)\sigma$ level persists. Notably, this lower flux level is compatible with a DM interpretation, as illustrated by the solid green curve in Fig. 2. Further detections will enable tighter constraints on the neutrino flux and, by extension, on models of DM origin. The energy spectrum of the observed neutrinos is particularly critical for disentangling astrophysical and nonastrophysical sources. Astrophysical sources are typically expected to produce a power-law spectrum, often correlated with UHE cosmic rays and UHE gamma rays. In contrast, DM-induced spectra can exhibit distinct features, such as the spectral spike shown in Fig. 2, which is generally not anticipated from conventional astrophysical sources. Nevertheless, future detection of more UHE neutrinos across a broad energy range will help resolve these UHE sources.

IV. DARK MATTER GENESIS

DM $N_{1(3)}$ at PeV scale can be produced via freeze-in through the following mechanisms: (i) the on-shell decay of Z', provided that $M_{Z'} > 2M_{1(3)}$; (ii) the on-shell decay of ϕ, if $m_\phi > 2M_{1(3)}$; and (iii) $2 \to 2$ scattering of thermal bath particles mediated by Z' (see Appendixes B and C for detailed expressions). The coupling strength g_X must be sufficiently small to ensure nonthermal DM production via freeze-in. Consequently, Z' never attains thermal equilibrium, and its comoving number density must be determined by solving a set of coupled Boltzmann equations (see Appendix D for details). We assume the mixing between ϕ and h is negligibly small, and, therefore, ϕ-mediated scatterings and its decay into SM particles will be highly suppressed resulting not to consider their effects [64–66]. As a result, ϕ—which remains part of the thermal bath—predominantly decays into RHNs and Z' in pairs. To fit the observed DM relic density, it is required that $y_0 M_{1(3)} = \Omega h^2 \frac{1}{s_0}\frac{\rho_c}{h^2} \simeq 4.3 \times 10^{-10}$ GeV, where $y_0 \equiv y_{N_{1(3)}}(z \to \infty)$ is the present DM yield. We use the critical energy density $\rho_c \simeq 1.05 \times 10^{-5} h^2$ GeV/cm^3, present entropy density $s_0 \simeq 2.69 \times 10^3$ cm^{-3} [67] and DM relic abundance $\Omega h^2 \simeq 0.12$, with $h \simeq H_0/100$ (km/s/Mpc) being the reduced Hubble rate, where $H_0 \simeq 67.4 \pm 0.5$ km/s/Mpc is the current Hubble rate [68].

The DM yield as a function of $z = M_{1(3)}/T$ is shown in Fig. 4. In the present scenario, Z' is always produced from the on-shell two-body decay $\phi \to Z'Z'$; therefore, in all cases we consider $m_\phi > 2M_{Z'}$. For $M_{1(3)} < M_{Z'}/2$, as well as $M_{1(3)} < m_\phi/2$, DM is dominantly produced from decays; hence, an extremely tiny g_X is required to satisfy the DM abundance. This situation is considered in the top left panel. The DM production shows a nontrivial dynamics here. This is because both Z' and DM yield builds up from ϕ decay. Since ϕ decays (green dot-dashed curve) earlier compared to Z' (red dashed curve), hence the final DM abundance is set by Z' decay. As a result, we notice a tiny bump at $z \sim 3 \times 10^7$, where Z' decay is completed, saturating the DM relic. In the top right panel, DM production dominantly takes place via ϕ decay since $M_{1(3)} < m_\phi/2$ but $M_{1(3)} > M_{Z'}$. Once again, we see g_X needs to be very feeble to produce the observed DM abundance. It is important to mention that $g_X = 10^{-15}$ requires a Planckian v_Φ in order to satisfy $M_{Z'} \geq 1$ TeV and, thus, is forbidden. For DM production entirely via Z'-mediated scattering, one requires $M_{1(3)} > M_{Z'}, m_\phi$. Here the DM freezes in at $z \simeq 1$, as shown in the bottom panel. This is the typical IR feature of freeze-in, where the freeze-in happens at $T = \max[M_{Z'}, M_{1(3)}]$. Note that in this case it is possible to have a much larger g_X, since scattering channels have a g_X^4 dependence, compared to g_X^2 dependence for decays.

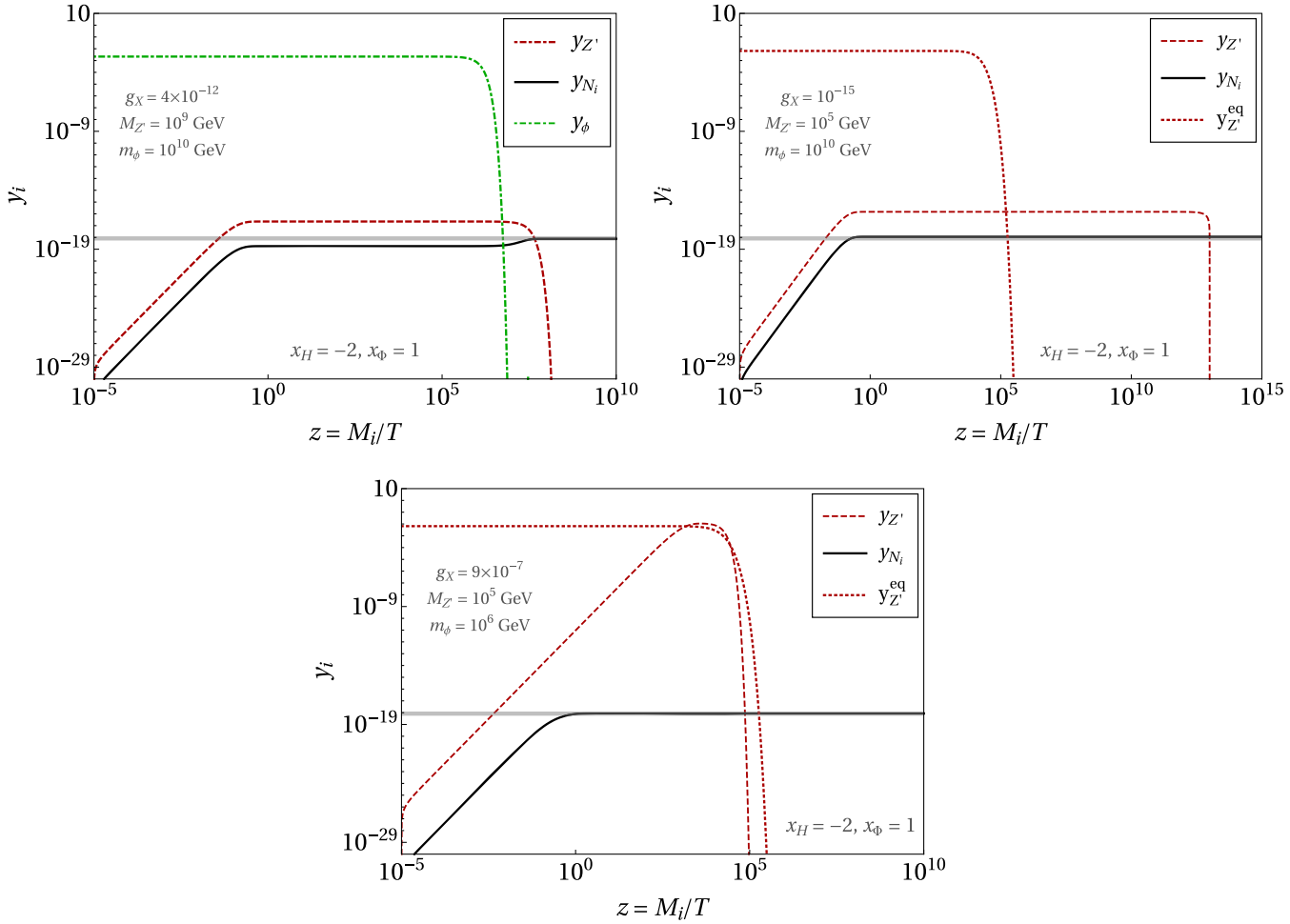


FIG. 4. Evolution of DM yield (black solid curve), as a function of $z = m_{\nu_\alpha}/T$ with $M_{1(3)} = 440$ PeV for NH (IH) case taking $x_H = -2, x_\Phi = 1$ where DM is dominantly produced from the decays of both Z' and ϕ (top left), via ϕ decay (top right) and purely from Z'-mediated scattering (bottom).

V. GW SPECTRUM FROM COSMIC STRINGS

The primary mechanism of energy dissipation from CS is GW emission from oscillating loops, as demonstrated by numerical simulations based on the Nambu-Goto action [69,70]. The corresponding energy loss rate is given by [71]

$$P_{\rm GW} = \frac{G}{5}(\dddot{Q})^2, \tag{18}$$

where Q represents the quadrupole moment of the oscillating loop and its third time derivative scales as $\dddot{Q} \propto \mu$. Consequently, the energy loss rate follows as

$$\frac{dE}{dt} = -\Gamma G\mu^2, \tag{19}$$

where $\Gamma \approx 50$ [72]. Due to the emission of GWs, the loop undergoes a gradual reduction in length from its initial value $l_i = \alpha t_i$ at the formation time t_i, evolving as

$$l(t) = \alpha t_i - \Gamma G\mu(t - t_i), \tag{20}$$

where α denotes the loop size parameter, which simulations suggest is approximately $\alpha \approx 0.1$ [73,74]. The total energy radiated by a loop is distributed among a series of normal mode oscillations, characterized by discrete frequencies

$$f_k = \frac{2k}{l(t)}, \tag{21}$$

where k represents the mode number $(k = 1, 2, 3, \ldots, \infty)$. The GW spectral density is expressed as

$$\Omega_{\rm GW}(t_0, f) = \frac{f}{\rho_c}\frac{d\rho_{\rm GW}(t_0, f)}{df} = \sum_k \Omega_{\rm GW}^{(k)}(t_0, f), \tag{22}$$

where f and t_0 denote the present-day frequency and cosmic time, respectively. Since GW energy density redshifts as a^{-4}, we obtain [73]

$$\frac{d\rho_{\rm GW}^{(k)}}{df} = \int_{t_F}^{t_0} \left[\frac{a(t_E)}{a(t_0)}\right]^4 P_{\rm GW}(t_E, f_k) \frac{dF}{df} dt_E, \quad (23)$$

where f_k denotes the frequency at emission (f_E) at cosmic time t_E, with t_F representing the loop formation epoch. The factor $\frac{dF}{df} = f[\frac{a(t_0)}{a(t_E)}]$ accounts for the redshift of the frequency. The power radiated by the loops is given by

$$P_{\rm GW}(t_E, f_k) = \frac{2k G\mu^2 \Gamma_k}{f[\frac{a(t_0)}{a(t_E)}]^2} n\left(t_E, \frac{2k}{f}\left[\frac{a(t_E)}{a(t_0)}\right]\right), \quad (24)$$

where Γ_k is defined as

$$\Gamma_k = \frac{\Gamma k^{-4/3}}{\sum_{m=1}^{\infty} m^{-4/3}}, \quad (25)$$

such that $\sum_k \Gamma_k = \Gamma$. The function n, number density of loops, depends on the background cosmology characterized by a scale factor $a \propto t^\beta$. Using the velocity-dependent one-scale model [75–77] and numerical simulations [73], the loop number density is given by

$$n(t_E, l_k(t_E)) = \frac{A_\beta}{\alpha} \frac{(\alpha + \Gamma G\mu)^{3(1-\beta)}}{[l_k(t_E) + \Gamma G\mu t_E]^{4-3\beta} t_E^{3\beta}}, \quad (26)$$

where A_β is a constant that depends on the cosmological background. The resulting GW spectrum is influenced by the small-scale structure of loops, which may feature cusps or kinks [78,79]. Here we assume that cusplike structures primarily govern the emitted GW spectrum.

Utilizing Eqs. (22)–(26), the present-day GW energy density for a given mode k is obtained as

$$\Omega_{\rm GW}^{(k)}(t_0, f) = \frac{2k G\mu^2 \Gamma_k}{f\rho_c} \int_{t_{\rm osc}}^{t_0} dt \left[\frac{a(t)}{a(t_0)}\right]^5 n(t, l_k), \quad (27)$$

where the integration extends from $t_{\rm osc}$, the epoch at which loops commence oscillations after being damped by thermal friction [80]. This damping phase is subdominant in its effect on the resulting GW spectrum.

For loops that form and radiate during the radiation-dominated era, the GW spectrum exhibits a characteristic flat plateau, with an amplitude given by

$$\Omega_{\rm GW}^{(k=1),\rm plateau}(f) = \frac{128\pi G\mu}{9\zeta(4/3)} \frac{A_r}{\epsilon_r} \Omega_r [(1+\epsilon_r)^{3/2} - 1], \quad (28)$$

where $\epsilon_r = \alpha/\Gamma G\mu$ and $A_r = 0.54$ [77] for the radiation-dominated universe.

VI. RESULTS AND DISCUSSIONS

In Fig. 5 we show the relic density allowed parameter space for a 440 PeV DM. The thick and dashed contours correspond to $x_H = \{-2, 0\}$, respectively. We show the

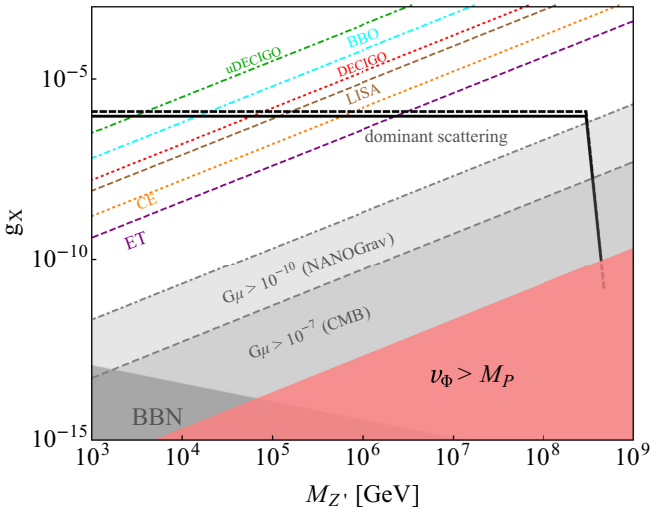


FIG. 5. Contours of right relic abundance for a 440 PeV DM, shown by the solid and dashed black curves, for $x_H = \{-2, 0\}$. Along the horizontal lines Z'-mediated scattering dominates. The diagonal dashed lines correspond to the sensitivity reaches of several futuristic GW detectors. The shaded regions are disallowed from BBN bound on Z' lifetime, requiring $\tau_{Z'} \gtrsim 1$ sec, Planckian VEV values, CMB and NANOGrav bounds on CS tension. DM production dominantly from ϕ decay requires $v_\Phi > M_P$, hence *forbidden* in this scenario.

reach of proposed GW detectors: Big Bang Observer (BBO) [81,82], ultimate DECIGO (uDECIGO) [83,84], Laser Interferometer Space Antenna (LISA) [85], the Cosmic Explorer (CE) [86], and the Einstein Telescope (ET) [87–90] in probing the parameter space, depending on v_Φ. The light gray shaded region in the bottom left corner corresponds to $\tau_{Z'} = 1/\Gamma_{Z'} > 1$ s, that can potentially perturb the predictions of big bang nucleosynthesis (BBN). The darker red shaded region in the bottom right corner demands (super-)Planckian v_Φ. Observations of the CMB impose an upper limit on the string tension, requiring $G\mu \lesssim 10^{-7}$ [91]. Under this constraint, the condition $\alpha \gg \Gamma G\mu$ holds, leading to $\Omega_{\rm GW}^{(k=1)}(f) \propto v_\Phi$. Recent results from NANOGrav [92] impose an even more stringent upper bound, limiting $G\mu \lesssim 10^{-10}$.

Now, along the horizontal branch of the black curves, the correct DM abundance is produced entirely via Z'-mediated scattering. Along these lines, we consider $m_\phi = 10^6$ GeV, ensuring $m_\phi < 2M_{1(3)}$ while maintaining $m_\phi > 2M_{Z'}$. For $M_{Z'} \simeq 5 \times 10^7$ GeV, we set $m_\phi = 10^9$ GeV, ensuring that the decay channel $\phi \to Z'Z'$ is kinematically allowed. Since now $m_\phi > 2M_{1(3)}$, all decay channels become accessible, thereby requiring an extremely small g_X, as observed in the top panel of Fig. 4. We find $g_X \simeq \{9 \times 10^{-7}, 10^{-6}\}$, corresponding to $x_H = \{-2, 0\}$ for DM production via Z' scattering being independent of neutrino hierarchy as the DM mass is the same in both cases. For dominant DM production from ϕ decay, $g_X \lesssim \mathcal{O}(10^{-15})$ is required for

$M_{Z'} \gtrsim 1$ TeV, which implies $v_\Phi \sim M_P$, thereby excluding this possibility. Since a similar bound is obtained for $x_H = 0$, we do not explicitly show this case. For DM production purely via Z'-mediated scattering, we note, in the present framework, KM3NeT provides a slightly stronger bound than IceCube, where latter demands a decaying DM of mass 4 PeV [93,94]. This can be understood from the fact that since in this case the final DM yield is largely independent of the mediator mass, hence one can write $(g_X^{\rm KM3}/g_X^{\rm ice}) \sim (4/440)^{1/4} \simeq 0.3$ for $x_H = 0$.

VII. CONCLUSIONS

The detection of a flux of UHE neutrinos by the deep-sea neutrino telescope KM3NeT opens a new avenue for investigating high-energy astrophysical sources, both Galactic and extra-Galactic. Additionally, it offers a powerful tool for constraining physics beyond the SM. This paper presents a minimal particle physics framework in which the origin of these high-energy neutrinos is linked to the decay of a PeV-scale fermionic DM candidate depending on neutrino mass hierarchy. This, in turn, imposes constraints on the mass and coupling of the new neutral gauge boson within the theory. Furthermore, we demonstrate that the viable DM parameter space, satisfying the KM3NeT events, lies within the sensitivity range of multiple gravitational wave detectors, highlighting a valuable complementarity in the quest for searching new physics.

ACKNOWLEDGMENTS

B. B. acknowledges fruitful discussions with Suruj Jyoti Das. P. S. thanks Nayan Das for sharing some data used in this work. The authors thank Latham Boyle for pointing out a crucial typo in the earlier version and for providing a useful reference.

DATA AVAILABILITY

Data are not publicly available. Data are available from the authors upon reasonable request.

APPENDIX A: NEUTRINO MASS

In order to generate the neutrino mass from the seesaw mechanism, the neutrino mass matrix can be written as

$$\mathcal{M}_\nu = \begin{pmatrix} 0 & M_D \\ M_D^T & M_N \end{pmatrix}. \tag{A1}$$

Assuming the hierarchy of $|M_{D_{ij}}/M_{N_\beta}| \ll 1$, we diagonalize the neutrino mass matrix to obtain the nonzero neutrino mass eigenvalue of light Majorana neutrino as

$$m_\nu \simeq -M_D M_N^{-1} M_D^T, \tag{A2}$$

which is the well-known seesaw formula. Due to the light-heavy neutrino mixing from the seesaw mechanism, a flavor eigenstate of light neutrino (ν_α) can be written as a linear combination of the mass eigenstates of light (ν_i) and heavy (N_i) neutrino:

$$\nu_\alpha \simeq \mathcal{U}_{\alpha i}\nu_i + V_{\alpha i} N_i, \tag{A3}$$

where $\mathcal{U}$, the PMNS matrix, is taken at the leading order after ignoring the nonunitarity effects for simplicity. Now we diagonalize the light neutrino mass matrix as

$$\mathcal{U}^T m_\nu \mathcal{U} = \mathrm{diag}(m_1, m_2, m_3), \tag{A4}$$

where PMNS matrix can be given by

$$\mathcal{U} = \begin{pmatrix} C_{12}C_{13} & S_{12}C_{13} & S_{13}e^{i\delta} \\ -S_{12}C_{23} - C_{12}S_{23}S_{13}e^{i\delta} & C_{12}C_{23} - S_{12}S_{23}S_{13}e^{i\delta} & S_{23}C_{13} \\ S_{12}C_{23} - C_{12}C_{23}S_{13}e^{i\delta} & -C_{12}S_{23} - S_{12}C_{23}S_{13}e^{i\delta} & C_{23}C_{13} \end{pmatrix} \begin{pmatrix} 1 & 0 & 0 \\ 0 & e^{i\rho_1} & 0 \\ 0 & 0 & e^{i\rho_2} \end{pmatrix} \tag{A5}$$

with $C_{ij} = \cos\theta_{ij}$, $S_{ij} = \sin\theta_{ij}$, $\delta(\rho_{1,2})$ is the Dirac (Majorana) CP phase. In this analysis we adopt neutrino oscillation data as $\sin^2 2\theta_{13} = 0.092$, $\sin^2 2\theta_{12} = 0.87$, $\sin^2 2\theta_{23} = 1.0$, $\Delta m^2_{12} = m_2^2 - m_1^2 = 7.6 \times 10^{-5}$ eV^2, and $|\Delta m^2_{23}| = |m_3^2 - m_2^2| = 2.4 \times 10^{-3}$ eV^2 from [41] for the NH and IH cases. Now we write the mixing between the light and heavy neutrino mass eigenstates in the seesaw scenario following general parametrization as

$$V^{\rm NH/IH} = \mathcal{U}^* \sqrt{D^{\rm NH/IH}}\,\mathcal{O}\sqrt{M_N^{-1}}, \tag{A6}$$

where $\mathcal{O}$ is a general orthogonal matrix:

$$\mathcal{O} = \begin{pmatrix} 1 & 0 & 0 \\ 0 & \cos x & \sin x \\ 0 & -\sin x & \cos x \end{pmatrix} \begin{pmatrix} \cos y & 0 & \sin y \\ 0 & 1 & 0 \\ -\sin y & 0 & \cos y \end{pmatrix} \times \begin{pmatrix} \cos z & \sin z & 0 \\ -\sin z & \cos z & 0 \\ 0 & 0 & 1 \end{pmatrix} \tag{A7}$$

with the angles x, y, z being complex numbers, and $D_{\rm NH/IH}$ is the light neutrino mass eigenvalue matrix

$$D^{\rm NH} = {\rm diag}(m_{\rm lightest}, m_2^{\rm NH}, m_3^{\rm NH}),$$
$$D^{\rm IH} = {\rm diag}(m_1^{\rm IH}, m_2^{\rm IH}, m_{\rm lightest}) \quad \text{(A8)}$$

with $m_2^{\rm NH} = \sqrt{\Delta m_{12}^2 + m_{\rm lightest}^2}$, $m_3^{\rm NH} = \sqrt{\Delta m_{23}^2 + (m_2^{\rm NH})^2}$, $m_2^{\rm IH} = \sqrt{\Delta m_{23}^2 + m_{\rm lightest}^2}$ and $m_1^{\rm IH} = \sqrt{(m_2^{\rm IH})^2 - \Delta m_{12}^2}$. In both cases, the RHN mass matrix is defined as $M_N = {\rm diag}(M_{N_1}, M_{N_2}, M_{N_3})$. Hence, the mixing matrix V in Eq. (7) becomes a function of $\rho_{1,2}$, $m_{\rm lightest}$, M_{N_β} ($\beta = 1$, 2, 3), the three complex angles and neutrino oscillation data. For a simple parametrization one can consider that x, y, $z = 0$ making $\mathcal{O}$ an identity matrix. Now the modified charged-current (CC) interaction in the lepton sector can be written as

$$\mathcal{L}_{\rm CC} = -\frac{g}{\sqrt{2}} W_\mu \overline{\ell} \gamma^\mu P_L [\mathcal{U}_{\alpha i} \nu_i + V_{\alpha i} N_i] + {\rm H.c.}, \quad \text{(A9)}$$

where g is the $SU(2)_L$ gauge coupling and the modified neutral-current (NC) interaction in the lepton sector will be

$$\mathcal{L}_{\rm NC} = -\frac{g}{2\cos\theta_w} Z_\mu [(\mathcal{U}^\dagger \mathcal{U})_{ij} \bar{\nu}_i \gamma^\mu P_L \nu_j + (\mathcal{U}^\dagger V)_{ki} \bar{\nu}_k \gamma^\mu P_L N_i + (V^\dagger V)_{mi} \bar{N}_m \gamma^\mu P_L N_i] + {\rm H.c.}, \quad \text{(A10)}$$

where θ_w is the weak mixing angle.

APPENDIX B: INTERACTIONS AND DECAY WIDTHS

Under the general $U(1)_X$ scenario left- and right-handed fermions interact differently with the Z' and the interaction Lagrangian manifest chiral scenario involving their general $U(1)_X$ charges. We write the interactions Lagrangian as

$$\mathcal{L} = -g_X (\bar{f} \gamma^\mu q_{f_L} P_L f + \bar{f} \gamma^\mu q_{f_R} P_R f) Z'_\mu, \quad \text{(B1)}$$

where $P_{L(R)} = (1 \mp \gamma_5)/2$ is the left- (right-)handed projections and $q_{f_{L(R)}}$ is the corresponding general $U(1)_X$ charge of the left- (right-)handed fermion $(f_{L(R)})$. The partial decay widths of Z' into a pair of charged fermions can be written as

$$\Gamma(Z' \to \bar{f} f) = N_C \frac{M_{Z'} g_X^2}{24\pi} \left[(q_{f_L}^2 + q_{f_R}^2) \left(1 - \frac{m_f^2}{M_{Z'}^2}\right) + 6 q_{f_L} q_{f_R} \frac{m_f^2}{M_{Z'}^2} \right] \left(1 - 4\frac{m_f^2}{M_{Z'}^2}\right)^{\frac{1}{2}}, \quad \text{(B2)}$$

where m_f is the mass of the SM fermions and $N_C = 1$ (3) is the color factor for the SM leptons (quarks). For heavy Z' in the TeV scale and above, the effect of the SM masses can be neglected. The partial decay width of Z' into a pair of light neutrinos (ν_L) can be written as

$$\Gamma(Z' \to \nu\nu) = \frac{M_{Z'} g_X^2}{24\pi} q_{\ell_L}^2, \quad \text{(B3)}$$

neglecting the tiny light neutrino mass and q_{ℓ_L} is the $U(1)_X$ charge of the SM lepton doublets. The Z' gauge boson can decay into a pair of heavy Majorana neutrinos if $M_{Z'} > M_{N_\beta}/2$. The kinematically allowed partial decay width of Z' into one generation of heavy neutrino pair can be given by

$$\Gamma(Z' \to N_\beta N_\beta) = \frac{M_{Z'} g_X^2}{24\pi} q_{N_R}^2 \left(1 - 4\frac{M_{N_\beta}^2}{M_{Z'}^2}\right)^{\frac{3}{2}}, \quad \text{(B4)}$$

where q_{N_R} is the general $U(1)_X$ charge of the heavy neutrinos. If we consider the scenario where $M_{N_\beta} > M_{Z'}/2$, then $Z' \to N_\beta N_\beta$ mode will be absent. In addition we write the dominant decay rates of the BSM scalar ϕ into a pair of Z' from the kinetic term and into a pair of RHNs from the Yukawa interaction as

$$\Gamma_{\phi \to Z'Z'} = \frac{g_X^2}{8\pi r^4} \frac{M_{Z'}^2}{m_\phi} \sqrt{1 - 4r^2} (12r^4 - 4r^2 + 1), \quad \text{(B5)}$$

$$\Gamma_{\phi \to N_\beta N_\beta} = \frac{g_X^2}{2\pi} \left(\frac{M_{N_\beta}}{M_{Z'}}\right)^2 m_\phi \left(1 - \frac{4M_{N_\beta}^2}{m_\phi^2}\right)^{3/2}, \quad \text{(B6)}$$

where $r = M_{Z'}/m_\phi$.

APPENDIX C: DM PRODUCTION CROSS SECTION

For charged lepton initial states,

$$\sigma(s)_{\ell^+\ell^- \to \rm DMDM} \simeq \frac{g_X^4}{96\pi[(s - M_{Z'}^2)^2 + \Gamma_{Z'}^2 M_{Z'}^2]} \sqrt{1 - \frac{4M_{N_1}^2}{s}} x_\Phi^2 \times \frac{(s - 4M_{N_1}^2)(5x_H^2 + 12 x_H x_\Phi + 8x_\Phi^2)}{2}. \quad \text{(C1)}$$

For light neutrino initial states,

$$\sigma(s)_{\nu\nu \to \rm DMDM} \simeq \frac{g_X^4}{48\pi[(s - M_{Z'}^2)^2 + \Gamma_{Z'}^2 M_{Z'}^2]} \sqrt{1 - \frac{4M_{N_1}^2}{s}} x_\Phi^2 \times \frac{(s - 4M_{N_1}^2)(x_H + 2x_\Phi)^2}{4}. \quad \text{(C2)}$$

For up-quark initial states,

$$\sigma(s)_{uu \to \rm DMDM} \simeq x_\Phi^2 \frac{(s - 4M_{N_1}^2)(17x_H^2 + 20 x_H x_\Phi + 8x_\Phi^2)}{2}. \quad \text{(C3)}$$

For down-quark initial states,

$$\sigma(s)_{dd\to\mathrm{DMDM}} \simeq x_\Phi^2 \frac{(s-4M_{N_1}^2)(5x_H^2-4x_Hx_\Phi+8x_\Phi^2)}{2}. \tag{C4}$$

APPENDIX D: BOLTZMANN EQUATIONS

The coupled Boltzmann equations for freeze-in production of the DM read

$$\begin{aligned}
\frac{dy_\phi}{dz} &= -\frac{z}{\mathcal{H}}\langle\Gamma_\phi\rangle y_{\mathrm{eq}}^\phi + \frac{s}{\mathcal{H}}\frac{1}{z^2}\langle\sigma v\rangle_{\mathrm{SMSM}\to\phi\phi}(y_{\mathrm{eq}}^\phi)^2,\\
\frac{dy_{Z'}}{dz} &= -\frac{z}{\mathcal{H}}\langle\Gamma_{Z'}\rangle y_{Z'} + \frac{z}{\mathcal{H}}\langle\Gamma_{\phi\to Z'Z'}\rangle(y_{\mathrm{eq}}^\phi - y_{Z'}),\\
\frac{dy_{N_1}}{dz} &= \frac{z}{\mathcal{H}}\langle\Gamma_{Z'\to N_1N_1}\rangle y_{Z'} + \frac{z}{\mathcal{H}}\langle\Gamma_{\phi\to N_1N_1}\rangle y_{\mathrm{eq}}^\phi\\
&\quad + \frac{s}{\mathcal{H}}\frac{1}{z^2}\langle\sigma v\rangle_{\mathrm{SMSM}\to N_1N_1} y_{\mathrm{eq}}^2,
\end{aligned} \tag{D1}$$

where $y_i \equiv n_i/s$ is the yield of a certain species i, with

$$y_j^{\mathrm{eq}} = \frac{45}{4\pi^4}\frac{g_j}{g_{\star s}} z^2 K_2[z] \tag{D2}$$

the equilibrium yield, with g_j being the degrees of freedom for the corresponding j particle and $z = M_1/T$ is a dimensionless variable. Here, $\mathcal{H} = (\pi/3)\sqrt{g_\star/10}(T^2/M_P)$ is the Hubble parameter for a standard radiation-dominated universe and $s = (2\pi^2/45)g_{\star s}(T)T^3$ is the entropy density. The number of relativistic degrees of freedom in the bath corresponding to energy density and entropy density are tracked by $g_\star(T)$ and $g_{\star s}(T)$, respectively. At temperatures well above the QCD phase transition we have $g_\star(T) \simeq g_{\star s}(T) \approx 106$. The thermally averaged decay rate is given by

$$\langle\Gamma_{\phi\to jj}\rangle = \frac{K_1(z)}{K_2(z)} \times \Gamma_{\phi\to jj}, \tag{D3}$$

with $z = M_1/T$ and j represents the final state particle.

[1] S. Aiello *et al.* (KM3NeT Collaboration), Observation of an ultra-high-energy cosmic neutrino with KM3NeT, Nature (London) **638**, 376 (2025).
[2] O. Adriani *et al.* (KM3NeT, MessMapp Group, Fermi-LAT, Owens Valley Radio Observatory 40-m Telescope Group, SVOM Collaborations), Characterising candidate blazar counterparts of the ultra-high-energy event KM3-230213A, arXiv:2502.08484.
[3] O. Adriani *et al.* (KM3NeT Collaboration), On the potential galactic origin of the ultra-high-energy event KM3-230213A, arXiv:2502.08387.
[4] O. Adriani *et al.* (KM3NeT Collaboration), On the potential cosmogenic origin of the ultra-high-energy event KM3-230213A, Astrophys. J. Lett. **984**, L41 (2025).
[5] K. Greisen, End to the cosmic ray spectrum?, Phys. Rev. Lett. **16**, 748 (1966).
[6] G. T. Zatsepin and V. A. Kuzmin, Upper limit of the spectrum of cosmic rays, JETP Lett. **4**, 78 (1966).
[7] G. Gelmini, O. E. Kalashev, and D. V. Semikoz, GZK photons as ultra high energy cosmic rays, J. Exp. Theor. Phys. **106**, 1061 (2008).
[8] R. Aloisio, D. Boncioli, A. di Matteo, A. F. Grillo, S. Petrera, and F. Salamida, Cosmogenic neutrinos and ultra-high energy cosmic ray models, J. Cosmol. Astropart. Phys. 10 (2015) 006.
[9] G. B. Gelmini, O. Kalashev, and D. Semikoz, Upper limit on the diffuse radio background from GZK photon observation, Universe **8**, 402 (2022).
[10] S. Chakraborty, P. Mehta, and P. Sarmah, A relook at the GZK neutrino-photon connection: impact of extra-galactic radio background & UHECR properties, J. Cosmol. Astropart. Phys. 01 (2024) 058.
[11] S. W. Li, P. Machado, D. Naredo-Tuero, and T. Schwemberger, Clash of the Titans: Ultra-high energy KM3NeT event versus IceCube data, arXiv:2502.04508.
[12] O. Adriani *et al.* (KM3NeT Collaboration), The ultra-high-energy event KM3-230213A within the global neutrino landscape, Phys. Rev. X **15**, 031016 (2025).
[13] B. Barman, A. Das, S. Jyoti Das, and M. Merchand, Hunting for heavy Z' with IceCube neutrinos and gravitational waves, Phys. Rev. D **112**, 035035 (2025).
[14] A. Boccia and F. Iocco, A strike of luck: Could the KM3-230213A event be caused by an evaporating primordial black hole?, arXiv:2502.19245.
[15] D. Borah, N. Das, N. Okada, and P. Sarmah, Possible origin of the KM3-230213A neutrino event from dark matter decay, Phys. Rev. D **111**, 123022 (2025).
[16] V. Brdar and D. S. Chattopadhyay, Does the 220 PeV event at KM3NeT point to new physics?, arXiv:2502.21299.
[17] K. Kohri, P. K. Paul, and N. Sahu, Super heavy dark matter origin of the PeV neutrino event: KM3-230213A, Phys. Rev. D **112**, L031703 (2025).
[18] Y. Narita and W. Yin, Explaining the KM3-230213A detection without gamma-ray emission: Cosmic-ray dark radiation, arXiv:2503.07776.
[19] S. Jiang and F. P. Huang, Pseudo-goldstone dark matter from primordial black holes: Gravitational wave signatures and implications for KM3-230213A event at KM3NeT, J. Cosmol. Astropart. Phys. 06 (2025) 023.
[20] G. F. S. Alves, M. Hostert, and M. Pospelov, Neutron portal to ultra-high-energy neutrinos, arXiv:2503.14419.
[21] R. Wang and B.-Q. Ma, Association of 220 PeV neutrino KM3-230213A with gamma-ray bursts, Res. Notes AAS **9**, 65 (2025).

[22] Y.-M. Yang, X.-J. Lv, X.-J. Bi, and P.-F. Yin, Constraints on Lorentz invariance violation in neutrino sector from the ultra-high-energy event KM3-230213A, Phys. Rev. D **111**, 123037 (2025).
[23] K. Fang, F. Halzen, and D. Hooper, Cascaded gamma-ray emission associated with the KM3NeT ultra-high-energy event KM3-230213A, Astrophys. J. Lett. **982**, L16 (2025).
[24] P. Satunin, Ultra-high-energy event KM3-230213A constraints on Lorentz invariance violation in neutrino sector, Eur. Phys. J. C **85**, 545 (2025).
[25] T. A. Dzhatdoev, The blazar PKS 0605-085 as the origin of the KM3-230213A ultra high energy neutrino event, arXiv:2502.11434.
[26] A. Neronov, F. Oikonomou, and D. Semikoz, KM3-230213A: An ultra-high energy neutrino from a year-long astrophysical transient, arXiv:2502.12986.
[27] G. Amelino-Camelia, G. D'Amico, G. Fabiano, D. Frattulillo, G. Gubitosi, A. Moia, and G. Rosati, On testing in-vacuo dispersion with the most energetic neutrinos: KM3-230213A case study, Phys. Lett. B **868**, 139764 (2025).
[28] M. Crnogorčević, C. Blanco, and T. Linden, Looking for the γ-ray cascades of the KM3-230213A neutrino source, arXiv:2503.16606.
[29] Y. Jho, S. C. Park, and C. S. Shin, Superheavy supersymmetric dark matter for the origin of KM3NeT ultra-high energy signal, arXiv:2503.18737.
[30] A. P. Klipfel and D. I. Kaiser, Ultra-high-energy neutrinos from primordial black holes, arXiv:2503.19227.
[31] K.-Y. Choi, E. Lkhagvadorj, and S. Mahapatra, Cosmological origin of the KM3-230213A event and associated gravitational waves, arXiv:2503.22465.
[32] A. Das, N. Okada, and D. Raut, Enhanced pair production of heavy Majorana neutrinos at the LHC, Phys. Rev. D **97**, 115023 (2018).
[33] S. K. A., A. Das, G. Lambiase, T. Nomura, and Y. Orikasa, Probing chiral and flavored Z' from cosmic bursts through neutrino interactions, Eur. Phys. J. C **84**, 1224 (2024).
[34] P. Minkowski, $\mu \to e\gamma$ at a rate of one out of 10^9 muon decays?, Phys. Lett. **67B**, 421 (1977).
[35] T. Yanagida, Horizontal gauge symmetry and masses of neutrinos, Conf. Proc. C **7902131**, 95 (1979).
[36] M. Gell-Mann, P. Ramond, and R. Slansky, Complex spinors and unified theories, Conf. Proc. C **790927**, 315 (1979).
[37] R. N. Mohapatra and G. Senjanovic, Neutrino mass and spontaneous parity nonconservation, Phys. Rev. Lett. **44**, 912 (1980).
[38] J. Schechter and J. W. F. Valle, Neutrino masses in $SU(2) \times U(1)$ theories, Phys. Rev. D **22**, 2227 (1980).
[39] *Proceedings: Workshop on the Unified Theories and the Baryon Number in the Universe: Tsukuba, Japan, 1979*, edited by O. Sawada and A. Sugamoto (National Laboratory for High Energy Physics, Tsukuba, Japan, 1979).
[40] R. N. Mohapatra and G. Senjanovic, Neutrino masses and mixings in gauge models with spontaneous parity violation, Phys. Rev. D **23**, 165 (1981).
[41] S. Navas *et al.* (Particle Data Group Collaboration), Review of particle physics, Phys. Rev. D **110**, 030001 (2024).
[42] L. J. Hall, K. Jedamzik, J. March-Russell, and S. M. West, Freeze-in production of FIMP dark matter, J. High Energy Phys. 03 (2010) 080.
[43] L. Boyle, K. Finn, and N. Turok, *CPT*-symmetric universe, Phys. Rev. Lett. **121**, 251301 (2018).
[44] H. B. Nielsen and P. Olesen, Vortex line models for dual strings, Nucl. Phys. **B61**, 45 (1973).
[45] T. W. B. Kibble, Topology of cosmic domains and strings, J. Phys. A **9**, 1387 (1976).
[46] A. Babul, T. Piran, and D. N. Spergel, Bosonic superconducting cosmic strings. 1. Classical field theory solutions, Phys. Lett. B **202**, 307 (1988).
[47] A. Vilenkin and E. P. S. Shellard, *Cosmic Strings and Other Topological Defects* (Cambridge University Press, Cambridge, England, 2000), 7.
[48] J. A. Dror, T. Hiramatsu, K. Kohri, H. Murayama, and G. White, Testing the seesaw mechanism and leptogenesis with gravitational waves, Phys. Rev. Lett. **124**, 041804 (2020).
[49] A. Das, P. Konar, and S. Majhi, Production of heavy neutrino in next-to-leading order QCD at the LHC and beyond, J. High Energy Phys. 06 (2016) 019.
[50] J. F. Navarro, C. S. Frenk, and S. D. M. White, A universal density profile from hierarchical clustering, Astrophys. J. **490**, 493 (1997).
[51] J. F. Navarro, E. Hayashi, C. Power, A. Jenkins, C. S. Frenk, S. D. M. White, V. Springel, J. Stadel, and T. R. Quinn, The Inner structure of Lambda-CDM halos 3: Universality and asymptotic slopes, Mon. Not. R. Astron. Soc. **349**, 1039 (2004).
[52] J. Einasto and U. Haud, Galactic models with massive corona. I—Method. II—Galaxy, Astron. Astrophys. **223**, 89 (1989).
[53] A. W. Graham, D. Merritt, B. Moore, J. Diemand, and B. Terzic, Empirical models for dark matter halos. I. Nonparametric construction of density profiles and comparison with parametric models, Astron. J. **132**, 2685 (2006).
[54] A. Burkert, The structure of dark matter halos in dwarf galaxies, Astrophys. J. Lett. **447**, L25 (1995).
[55] F. W. Stecker, S. T. Scully, and M. A. Malkan, An empirical determination of the intergalactic background light from UV to FIR wavelengths using FIR deep galaxy surveys and the gamma-ray opacity of the universe, Astrophys. J. **827**, 6 (2016); **863**, 112(E) (2018).
[56] C. W. Bauer, N. L. Rodd, and B. R. Webber, Dark matter spectra from the electroweak to the Planck scale, J. High Energy Phys. 06 (2021) 121.
[57] Z. Cao *et al.* (LHAASO Collaboration), Measurement of ultra-high-energy diffuse gamma-ray emission of the galactic plane from 10 TeV to 1 PeV with LHAASO-KM2A, Phys. Rev. Lett. **131**, 151001 (2023).
[58] Y. A. Fomin, N. N. Kalmykov, I. S. Karpikov, G. V. Kulikov, M. Y. Kuznetsov, G. I. Rubtsov, V. P. Sulakov, and S. V. Troitsky, Constraints on the flux of $\sim(10^{16}$–$10^{17.5})$ eV cosmic photons from the EAS-MSU muon data, Phys. Rev. D **95**, 123011 (2017).
[59] A. Castellina (Pierre Auger Collaboration), Highlights from the Pierre Auger Observatory, Proc. Sci., ICRC2019 (**2021**) 004 [arXiv:1909.10791].
[60] H. Athar, M. Jezabek, and O. Yasuda, Effects of neutrino mixing on high-energy cosmic neutrino flux, Phys. Rev. D **62**, 103007 (2000).

[61] R. Abbasi *et al.* (IceCube Collaboration), The IceCube high-energy starting event sample: Description and flux characterization with 7.5 years of data, Phys. Rev. D **104**, 022002 (2021).
[62] M. G. Aartsen *et al.* (IceCube Collaboration), Differential limit on the extremely-high-energy cosmic neutrino flux in the presence of astrophysical background from nine years of IceCube data, Phys. Rev. D **98**, 062003 (2018).
[63] KM3NeT Collaboration, KM3NeT Official Website (2025), https://www.km3net.org/ (accessed: 2025-04-01).
[64] K. Kaneta, Z. Kang, and H.-S. Lee, Right-handed neutrino dark matter under the $B - -L$ gauge interaction, J. High Energy Phys. 02 (2017) 031.
[65] S. Eijima, O. Seto, and T. Shimomura, Revisiting sterile neutrino dark matter in gauged U(1)B-L model, Phys. Rev. D **106**, 103513 (2022).
[66] O. Seto, T. Shimomura, and Y. Uchida, Freeze-in sterile neutrino dark matter in feeble gauged $B - L$ model, J. High Energy Phys. 05 (2025) 147.
[67] R. L. Workman *et al.* (Particle Data Group Collaboration), Review of particle physics, Prog. Theor. Exp. Phys. **2022**, 083C01 (2022).
[68] N. Aghanim *et al.* (Planck Collaboration), Planck 2018 results. VI. Cosmological parameters, Astron. Astrophys. **641**, A6 (2020); **652**, C4(E) (2021).
[69] C. Ringeval, M. Sakellariadou, and F. Bouchet, Cosmological evolution of cosmic string loops, J. Cosmol. Astropart. Phys. 02 (2007) 023.
[70] J. J. Blanco-Pillado, K. D. Olum, and B. Shlaer, Large parallel cosmic string simulations: New results on loop production, Phys. Rev. D **83**, 083514 (2011).
[71] A. Vilenkin, Gravitational radiation from cosmic strings, Phys. Lett. **107B**, 47 (1981).
[72] T. Vachaspati and A. Vilenkin, Gravitational radiation from cosmic strings, Phys. Rev. D **31**, 3052 (1985).
[73] J. J. Blanco-Pillado, K. D. Olum, and B. Shlaer, The number of cosmic string loops, Phys. Rev. D **89**, 023512 (2014).
[74] J. J. Blanco-Pillado and K. D. Olum, Stochastic gravitational wave background from smoothed cosmic string loops, Phys. Rev. D **96**, 104046 (2017).
[75] C. J. A. P. Martins and E. P. S. Shellard, Quantitative string evolution, Phys. Rev. D **54**, 2535 (1996).
[76] C. J. A. P. Martins and E. P. S. Shellard, Extending the velocity dependent one scale string evolution model, Phys. Rev. D **65**, 043514 (2002).
[77] P. Auclair *et al.*, Probing the gravitational wave background from cosmic strings with LISA, J. Cosmol. Astropart. Phys. 04 (2020) 034.
[78] T. Damour and A. Vilenkin, Gravitational wave bursts from cusps and kinks on cosmic strings, Phys. Rev. D **64**, 064008 (2001).
[79] Y. Gouttenoire, G. Servant, and P. Simakachorn, Beyond the standard models with cosmic strings, J. Cosmol. Astropart. Phys. 07 (2020) 032.
[80] A. Vilenkin, Cosmic string dynamics with friction, Phys. Rev. D **43**, 1060 (1991).
[81] J. Crowder and N. J. Cornish, Beyond LISA: Exploring future gravitational wave missions, Phys. Rev. D **72**, 083005 (2005).
[82] V. Corbin and N. J. Cornish, Detecting the cosmic gravitational wave background with the big bang observer, Classical Quantum Gravity **23**, 2435 (2006).
[83] N. Seto, S. Kawamura, and T. Nakamura, Possibility of direct measurement of the acceleration of the universe using 0.1-Hz band laser interferometer gravitational wave antenna in space, Phys. Rev. Lett. **87**, 221103 (2001).
[84] H. Kudoh, A. Taruya, T. Hiramatsu, and Y. Himemoto, Detecting a gravitational-wave background with next-generation space interferometers, Phys. Rev. D **73**, 064006 (2006).
[85] P. Amaro-Seoane *et al.* (LISA Collaboration), Laser interferometer space antenna, arXiv:1702.00786.
[86] D. Reitze *et al.*, Cosmic explorer: The U.S. Contribution to gravitational-wave astronomy beyond LIGO, Bull. Am. Astron. Soc. **51**, 035 (2019).
[87] S. Hild *et al.*, Sensitivity studies for third-generation gravitational wave observatories, Classical Quantum Gravity **28**, 094013 (2011).
[88] M. Punturo *et al.*, The Einstein Telescope: A third-generation gravitational wave observatory, Classical Quantum Gravity **27**, 194002 (2010).
[89] B. Sathyaprakash *et al.*, Scientific objectives of Einstein telescope, Classical Quantum Gravity **29**, 124013 (2012); **30**, 079501(E) (2013).
[90] M. Maggiore *et al.*, Science case for the Einstein telescope, J. Cosmol. Astropart. Phys. 03 (2020) 050.
[91] T. Charnock, A. Avgoustidis, E. J. Copeland, and A. Moss, CMB constraints on cosmic strings and superstrings, Phys. Rev. D **93**, 123503 (2016).
[92] A. Afzal *et al.* (NANOGrav Collaboration), The NANOGrav 15 yr data set: Search for signals from new physics, Astrophys. J. Lett. **951**, L11 (2023); **971**, L27(E) (2024).
[93] A. Esmaili, S. K. Kang, and P. D. Serpico, IceCube events and decaying dark matter: Hints and constraints, J. Cosmol. Astropart. Phys. 12 (2014) 054.
[94] T. Higaki, R. Kitano, and R. Sato, Neutrinoful universe, J. High Energy Phys. 07 (2014) 044.